Measuring the 3D resolution of a micro-focus X-ray CT setup

Daniel Weiß[1], Qiang Shi[2], Christoph Kuhn[1]

[1]Carl Zeiss IMT GmbH,
73447 Oberkochen, Germany, e-mail: d.weiss@zeiss.de, c.kuhn@zeiss.de

[2]Karlsruhe Institute of Technology,
76131 Karlsruhe, Germany, e-mail: qiang8715@gmail.com

Abstract
One of the most important specifications of an industrial X-ray computed-tomography (CT) setup used for inspection is the 3-dimensional (3D) resolution that can be achieved in the volumetric image. Sometimes CT setups are evaluated in this regard using a 2D object such as the JIMA micro resolution chart; however, this approach measures the 2D resolution in a projection image and characterizes the performance of X-ray source and detector, not that of the complete CT setup. Depending on the CT acquisition trajectory, component alignment, and reconstruction artifacts, the 3D resolution might be considerably worse than the 2D resolution. It is therefore desirable to directly measure the 3D resolution. A micro-structured silicon phantom suitable for high-magnification X-ray CT with a micro-focus source, and containing structure widths down to one micrometer, has recently been made available by QRM GmbH. The phantom can be used to determine the axial and in-plane 3D resolution in several ways: "by eye" using bar and hole patterns as well as a "Siemens star", using a slanted-edge MTF as per ISO 12233, and by evaluation of the image contrast as a function of structure width. We report on experimental results with the new phantom and on the influence of CT correction methods on the 3D resolution.

Keywords: X-ray computed tomography, micro-focus, 3D resolution, Siemens star, slanted-edge MTF, ISO 12233

1 Introduction

For a cone-beam X-ray CT setup with a point source and a divergent projection geometry, a large range of object sizes can usually be imaged with a single setup. The CT setup is characterized by the size of the detector and its distance from the X-ray source. Large objects of almost detector size may be imaged close to the detector, and thus at low magnification, while small objects are imaged at high magnification and close to the X-ray source. The terms “small object” and “large object” are therefore to be understood in relation to the detector size.
When we are interested in the smallest object details that can be resolved for a given object, different constraints apply depending on the object size. This is owing to the image blurring introduced by the finite size of the X-ray source (see fig. 1). The blurring in the detector plane turns out to be

$$b = f * (M - 1), \qquad \text{(eq. 1)}$$

where f is the physical source size and M the magnification. Usually, the blurring needs to be smaller than the detector pixel pitch p in order to avoid a loss of resolution ($b < p$). For a large object close to the detector the magnification is close to 1, hence $b \ll f$, and a large source size is acceptable.

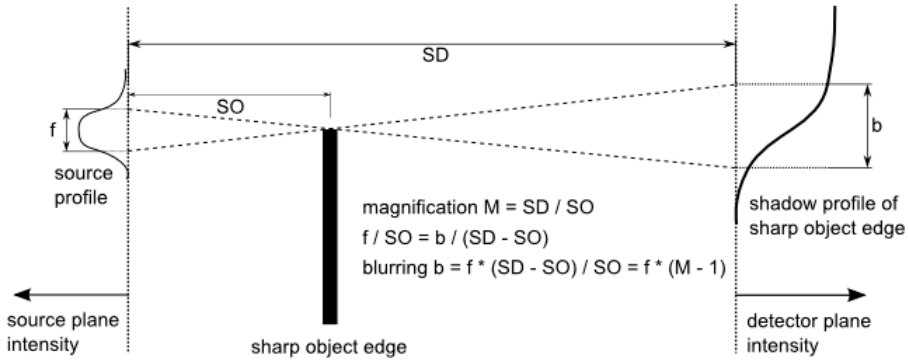

Figure 1: The influence of the source size f on the blurring b of the X-ray image depends on the magnification M.

At high magnification the source size is limited by the detector pixel pitch divided by the magnification ($f < p/(M-1) \approx p/M$). In this case an X-ray source with a physical source size of a few micrometers ("micro-focus") or even below ("nano-focus") can be used to advantage.
So on the one hand, image blurring caused by the finite source size limits the resolution in a digital radiograph, especially at high magnifications. On the other hand, the finite number of discrete resolution elements (pixels) in a digital detector also imposes a limitation on the minimum size of an object detail that is visible either in a radiograph or a volumetric image. For a large object, this limitation is more likely to be relevant than that of the source size.
There are additional physical effects that may limit the effective resolution, such as blurring caused by scattered radiation (either from the object, environment, or detector) and movement of one or more of the setup components during the exposure time. In the case of a volumetric image, the relative acquisition geometry of the individual X-ray projections needs to be known with high precision, otherwise high-spatial-frequency information from different projections may cancel each other out during reconstruction. An example for this is the effect of an error in the location of the projected rotation axis.
It is however at maximum magnification that a CT setup has its minimum voxel pitch and therefore the opportunity to demonstrate maximum resolution. In this case, it is preferable to evaluate the 3D resolution directly in a volumetric image, instead of attempting to extrapolate it from single radiographs.

2 Resolution test object "QRM Micro-CT Bar Pattern NANO"

A suitable test object ("phantom" in medical parlance) for evaluating the 3D resolution of a micro-focus CT setup was recently made available by QRM GmbH (Moehrendorf, Germany, [1]). The object consists of two silicon chips of size 3x3x0.66 mm placed at right angles, so that the axial and in-plane resolution can be determined at the same time (fig. 2.a). The protective housing has a diameter of ca. 5 mm, allowing for rotation through 360 degrees at high magnification. Each chip has a variety of patterns etched into one surface. Among these are horizontal and vertical bar patterns ranging from 1 to 10 micrometer line width, hole patterns with diameters between 1 and 10 µm, fan patterns and a "Siemens star" with an outermost line width of 17.5 µm (fig. 2.b). Since the structured layer is only 15 µm thick, compared to a chip thickness of 660 µm (fig. 2.d), the pattern contrast in single radiographs is very low and the chip is not suitable for determination of the 2D resolution, i.e., not a replacement for the JIMA chart [2].

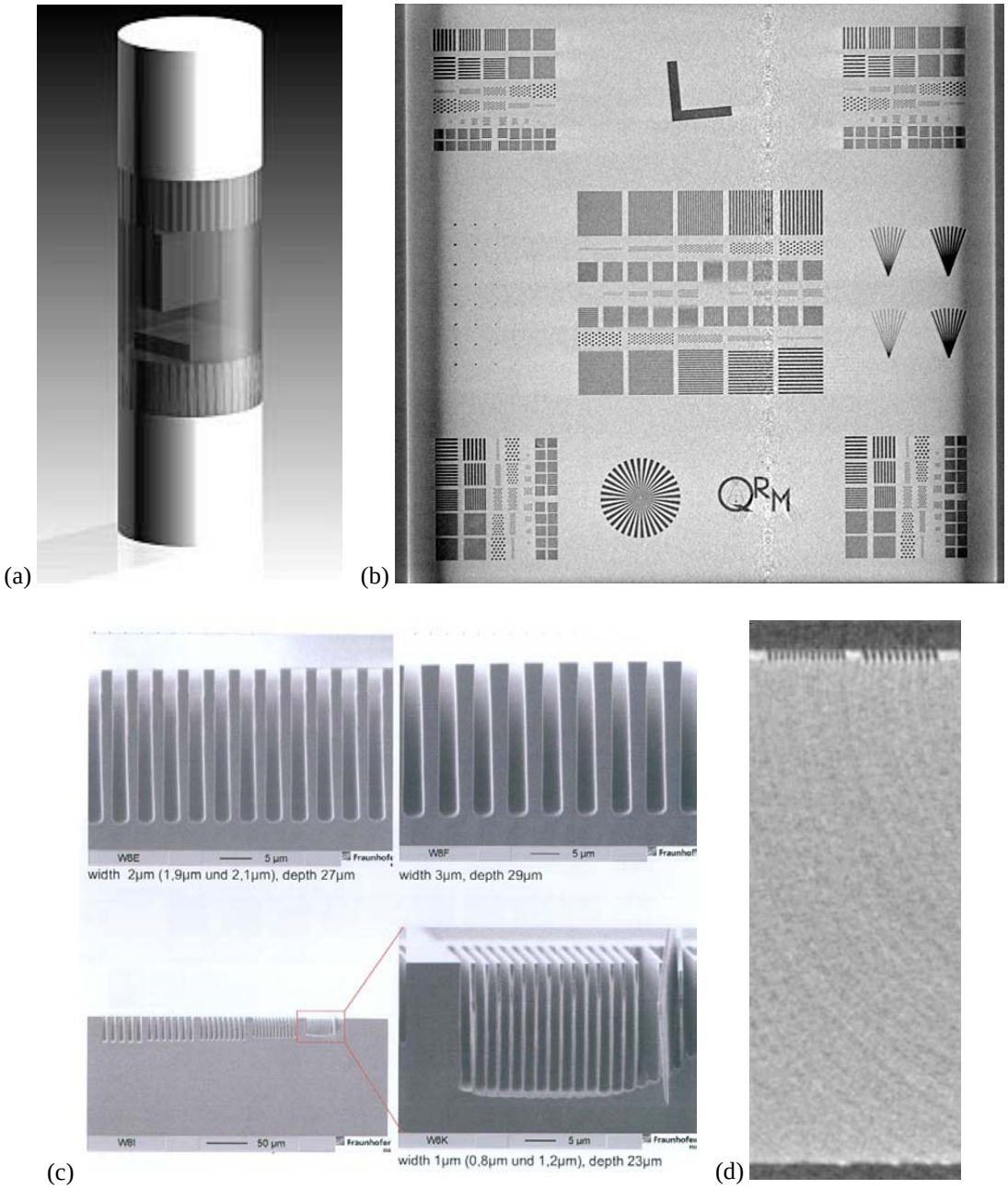

Figure 2: 3D resolution test object "QRM Micro-CT Bar Pattern NANO" consisting of two silicon chips placed at right angles inside a protective housing (a, image courtesy of QRM GmbH); reconstructed xz-slice through the upright chip showing the different patterns (b, the shading at the sides of the chip and the noisy vertical stripe are reconstruction artifacts); scanning electron micrograph showing the quality of prototype structuring even at high aspect-ratio (c, image courtesy of Fraunhofer IISB); reconstructed xy-slice through the chip showing the thin structured layer (15 µm) on one side of the chip (d).

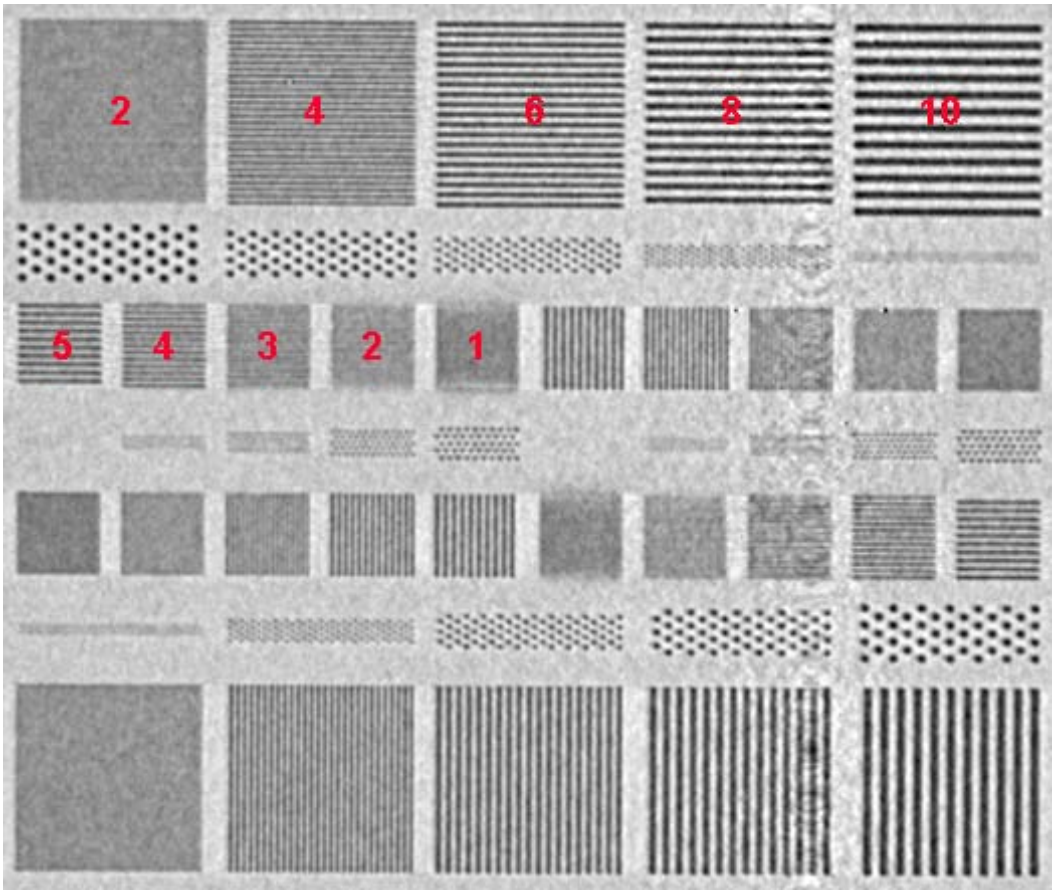

Figure 3: One reconstructed xz-slice of the phantom, showing bar and hole patterns with structure widths between 1 and 10 micrometers (voxel pitch 1.7 µm). The noisy vertical stripe at the right is caused by ring artifacts.

Since the structure width ranges from 1 to less than 20 µm, this resolution test is geared exclusively towards micro-focus CT setups (a different phantom spanning 5 – 150 µm structure width is also available, [3, 4]). The central section of the chip is shown in fig. 3. The CT measurement was performed on a METROTOM 800 (Carl Zeiss IMT GmbH) with a circular source trajectory (Feldkamp type, [5]) and a sealed micro-focus X-ray source L9181-02 (Hamamatsu Photonics) with an acceleration voltage of 60 kV and a beam current of 66 µA (200 µm Be window, no filters). For this source, the manufacturer specifies a focal spot size of 5 µm at 4 W [6]. The standard voxel pitch p/M at this magnification was 3.5 µm; however, the volumetric image was reconstructed with a voxel pitch of 1.7 µm (oversampling factor 2x) to avoid aliasing artifacts at the small structure widths.
As can be seen from fig. 3, the 3D resolution can be evaluated “by eye”. It is obvious that there is still discernible image contrast at 4 µm line width (both for vertical and horizontal bars), but not at 3 µm. The same observation holds true for the hole patterns.

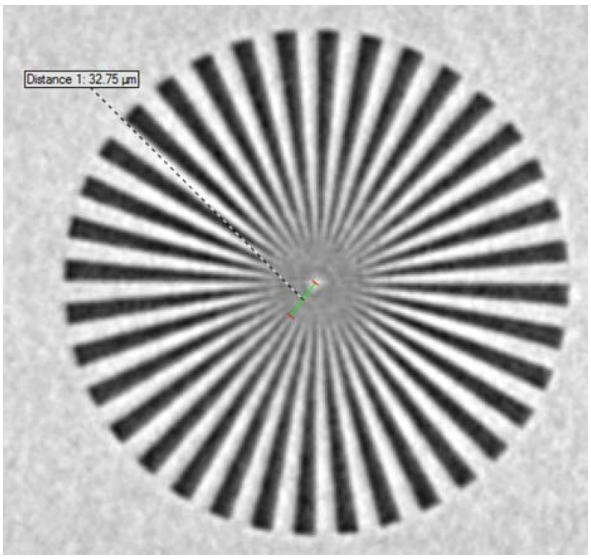

Figure 4: One reconstructed xz-slice of the phantom, showing the "Siemens star" and displaying image contrast for all directions in the xz-slice. The star pattern has an outermost line width of 17.5 µm at 200 µm radius, thus contrast cutoff occurs at approx. 3 µm line width (voxel pitch 1.7 µm).

3 Directional dependence observed on the "Siemens star"

The horizontal and vertical bar patterns shown in fig. 3 do not seem to indicate that the 3D resolution is strongly dependent on the direction of modulation. However, a better tool to investigate such directional dependence is the radial structure known as a "Siemens star".

In this case, the star pattern has a diameter of 400 µm and 36 pairs of bright and dark spokes, resulting in an outermost line width of 17.5 µm (fig. 4). As can be seen, the image contrast degrades from the rim to the center of the star pattern. A simple way of evaluating this image is to determine a radius at which the image contrast is degraded to zero, and compute the corresponding line width. The inner region displaying zero contrast appears to be roughly circular in form, so no directional dependence is apparent at this point.

In order to arrive at a quantitative evaluation of the star pattern, the local image contrast is calculated as a function of line width and direction. By determining minimum and maximum intensities for each period of the pattern and using the Michelson contrast definition

$$C = \frac{I_{max} - I_{min}}{I_{max} + I_{min}}, \qquad \text{(eq. 2)}$$

each position inside the star can be assigned a contrast value between 0 and 1 (fig. 5). The evaluation reveals that the image contrast does indeed depend on the direction of the structures: those spokes of the star pattern that are modulated in the z direction (vertical direction in the figure) exhibit a better contrast than those modulated in the x direction (horizontal direction in the figure), "better contrast" meaning that high contrast is maintained for smaller line widths. It is important to note that for the Feldkamp reconstruction the Ram-Lak row filter was used, not the Shepp-Logan filter or other filters that attenuate high frequencies. The decreased in-slice image contrast is thus not owing to Feldkamp row filtering.

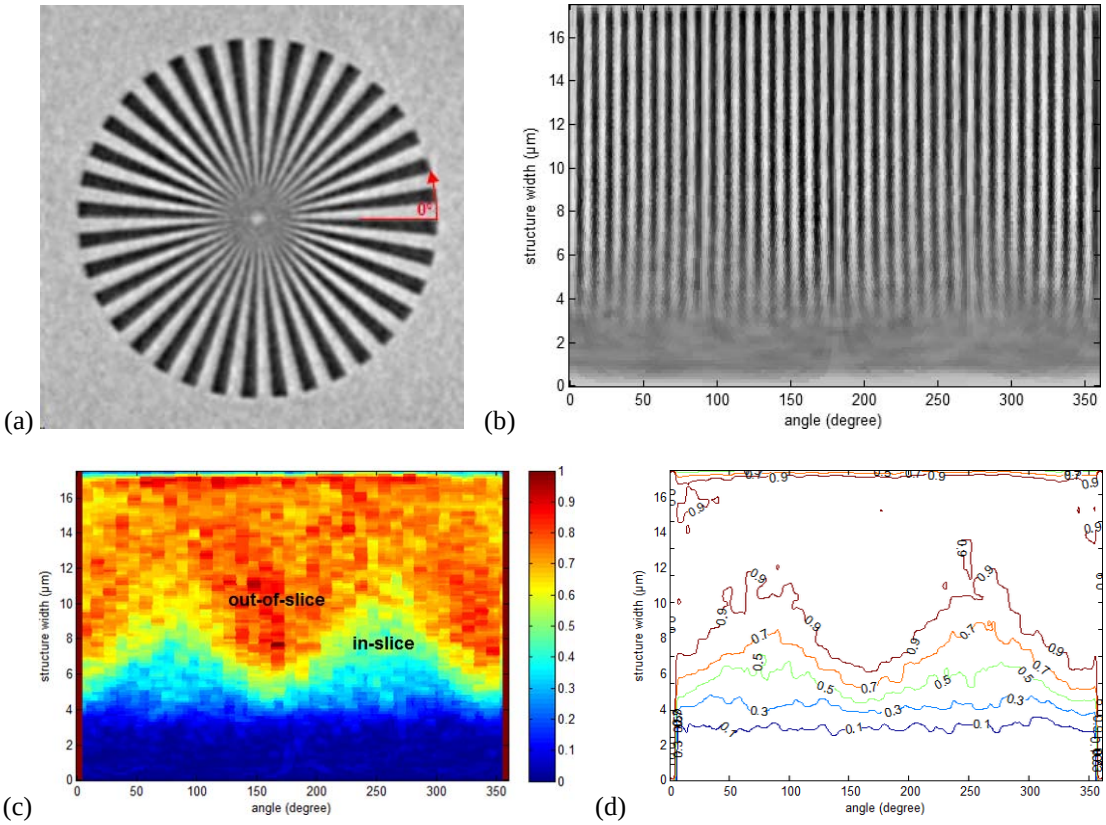

Figure 5: Evaluation of the star pattern to identify directional dependence of the image contrast. The original pattern (a) is "unrolled" by using nearest-neighbor interpolation on a polar coordinate system, in order to separate structure width and direction (b). Computation of the local Michelson contrast using a sliding horizontal window shows a directional dependence (c, d). Note that image contrast is better for structures modulated in the z direction (out-of-slice).

4 Influence of horizontal axis error

As an example of a CT artifact that affects 3D resolution, fig. 6 shows the influence of the horizontal axis error on image contrast. In order to reconstruct a volumetric image, the horizontal position of the projected rotation axis needs to be known. If this value has an error of more than one pixel, all object contours in xy-slices are accompanied by a double edge having a width of twice the error ("double-edge artifact"); if the error is below one pixel, the effect is perceived as blurring in the xy-slices.
However, in addition to the easily visible double edge, the horizontal axis error also affects the image contrast in xy-slices at all spatial frequencies in a characteristic manner. It may even lead to contrast enhancement for certain spatial frequencies, albeit at the cost of strongly decreased contrast at other frequencies (cf. fig. 6, last column).

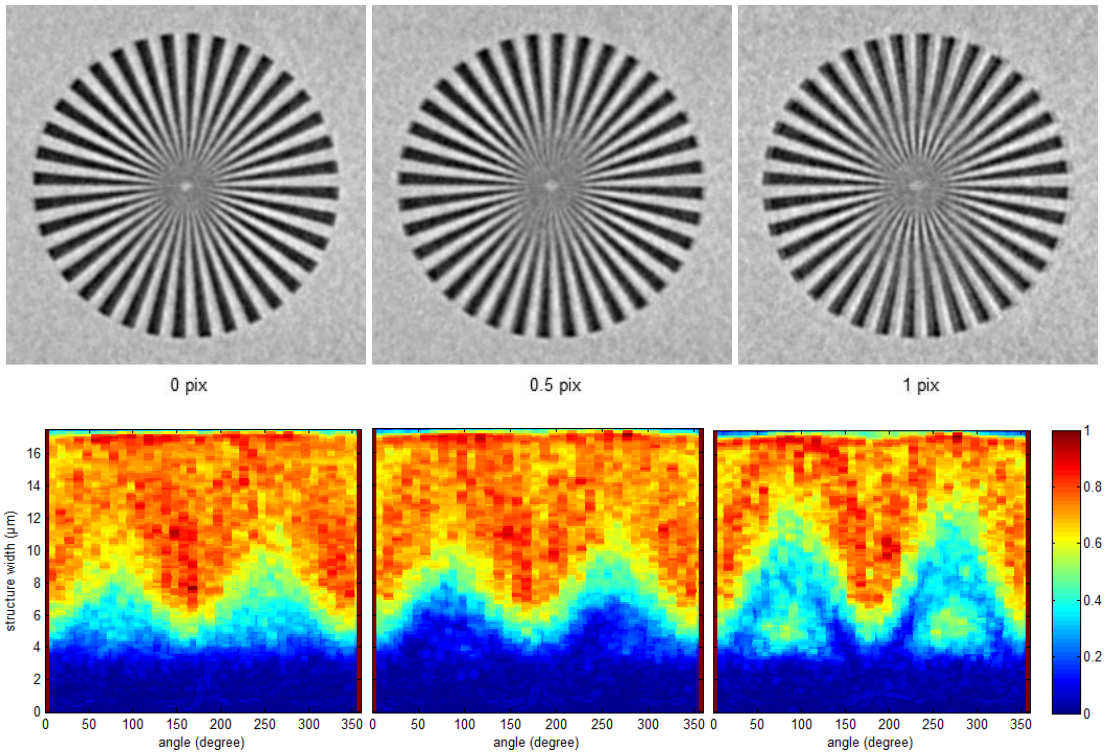

Figure 6: Influence of the horizontal axis error on image contrast. The first row shows the star pattern for an error of 0, 0.5, and 1 pixels, resp. The second row shows the local Michelson contrast. As expected, the horizontal axis error mostly affects the in-slice image contrast. For an error of 1 pixel, the in-slice contrast is no longer monotonically decreasing: a first contrast minimum occurs at 8 µm line width and is followed by a local maximum at 5 µm line width.

5 Slanted-edge MTF

It is interesting to compare the resolution results obtained so far with results provided by another method. The international standard ISO 15708 describes a technique to obtain the resolution from the volumetric image of a cylinder [7]. It does so by extracting the edge response function and, via computation of the line spread function (LSF), arrives at the modulation transfer function (MTF). In order to provide a single number for the 3D resolution, it is customary to specify the spatial frequency at which the (normalized) modulation transfer has dropped to 10 percent.

While the QRM phantom is not cylindrical, the surface of the Si chip provides an edge of high straightness and smoothness which can be used to perform an essentially equivalent evaluation. Described in ISO standard 12233 [8], this evaluation is known as a “slanted-edge MTF” and is in widespread use for optical systems such as lenses and cameras. For this paper, an implementation by P. Granton was used [9]. An advantage of CT is that the tilt angle of the edge can be set arbitrarily as a reconstruction parameter; here, a tilt angle of 4 degrees was used (fig. 7).

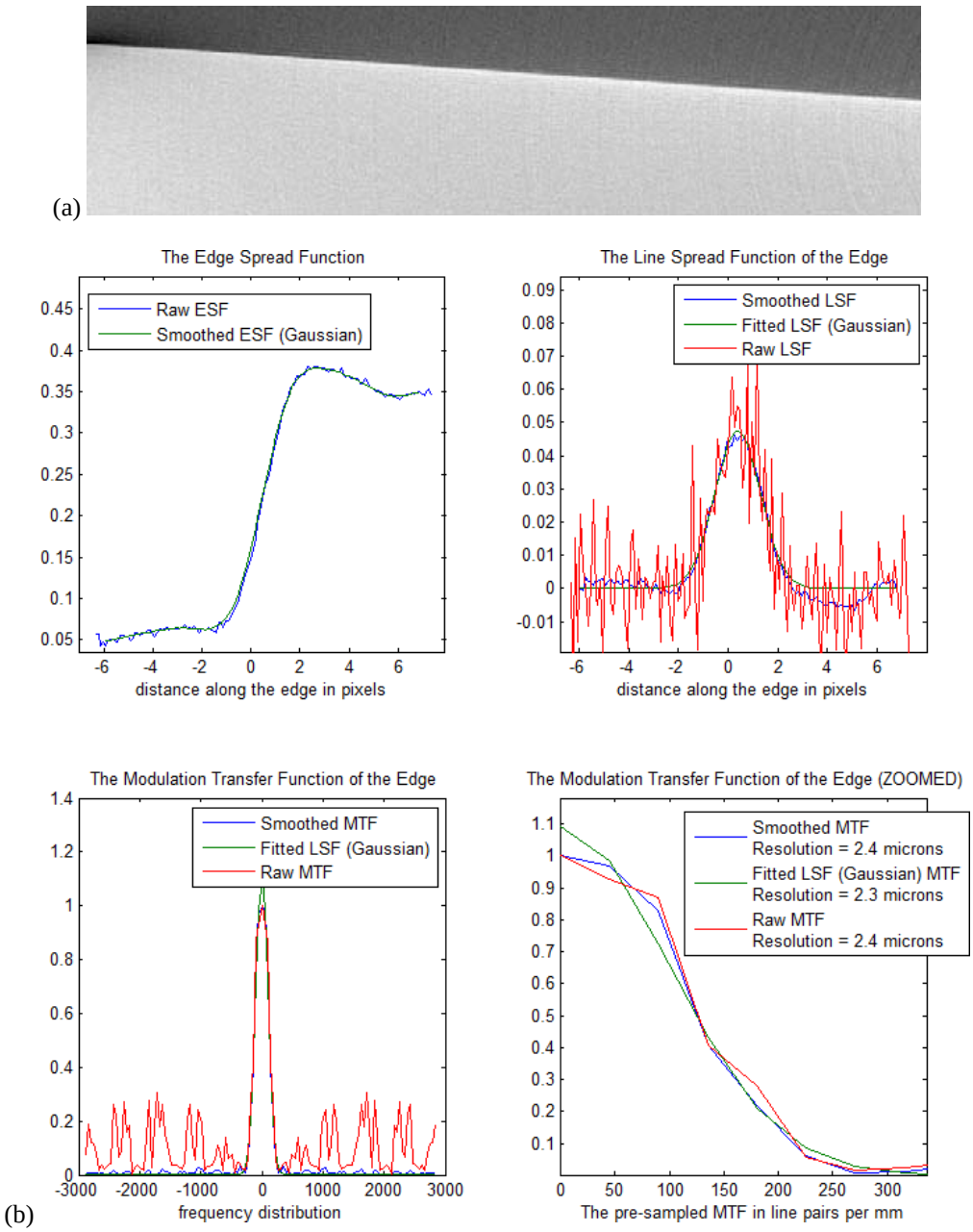

Figure 7: Slanted-edge MTF determination according to ISO 12233 as implemented in [9]. An unstructured region of the Si chip surface was averaged over 80 xy-slices to provide a low-noise edge with 4° tilt (a). MTF calculation consists of creating an oversampled (10x) representation of the edge spread function ESF (b, upper left), calculating the line spread function LSF as the derivative of the ESF (b, upper right), and computing the MTF as the Fourier transform of the LSF (b, lower left and right). Corresponding to the voxel pitch of 1.73 µm, the Nyquist frequency is 289 lp/mm. Note that smoothing the ESF and fitting the LSF with a Gaussian function provides two further estimates of the MTF.

In order to preserve the spatial frequency distribution inherent in the image data, the edge spread function (ESF) is created by binning voxel values according to their distance from the edge, rather than using any form of interpolation and resampling. In the implementation used here, the resulting ESF is also smoothed for further processing. Additionally, the LSF is fitted with a Gaussian function. This preserves the overall form of the edge gradient quite well, but suppresses artifacts away from the main peak. An additional benefit is that the Fourier transform of the fit Gaussian is also Gaussian and thus monotonically decreasing, so than normalization at 0 lp/mm is always possible. Especially for cylinder evaluation as per ISO 15708, beam hardening often causes a maximum MTF value at non-zero spatial frequency. In this case, the three MTF estimates agree quite well, yielding a 10%-value corresponding to approx. 2.4 µm line width.

10 Summary and outlook

We have evaluated a new test object made from micro-structured silicon that is suitable for the determination of 3D resolution in micro-focus X-ray computed-tomography setups. The object permits an assessment of the resolution both “by eye” through various bar and hole patterns, as well as by quantitative evaluation of the image contrast. Additionally, MTF determination as per ISO 12233 is possible.

The low attenuation of the resolution test object material (Si) somewhat restricts the applicability of the results to high-attenuation objects. An alternative test object suitable for high-kV X-ray CT setups would therefore be required, if and when comparable structuring capabilities for high-attenuation materials become available.

Acknowledgements

We would like to thank Oliver Langner of QRM GmbH for helpful discussions about the phantom and for providing additional information about the quality of the Si structuring.

References

[1] http://www.qrm.de/content/products/microct/microct_barpattern_nano.htm, retrieved June 5th, 2012.

[2] http://www.jima.jp/content/pdf/rt_ct-02cata02.pdf, retrieved June 5th, 2012.

[3] http://www.qrm.de/content/products/microct/microct_barpattern.htm, retrieved June 5th, 2012.

[4] Langner, O., Karolczak, M., Rattmann, G., Kalender, W., “Bar and Point Test Patterns Generated by Dry-Etching for Measurement of High Spatial Resolution in Micro-CT”, World Congress on Medical Physics and Biomedical Engineering, Munich, Germany, September 7 – 12, 2009.

[5] Feldkamp, L.A., Davis, L.C., Kress, J.W., "Practical cone-beam algorithm", J. Opt. Soc. Am. A 1, pp. 612-619, 1984.

[6] 130kV Microfocus X-ray source L9181-02, Instruction manual, Hamamatsu Photonics K. K., Electron tube division, 2007.

[7] International standard ISO 15708-1 “Non-destructive testing - Radiation methods - Computed tomography”, first edition 2002-06-01, section 7.3 “Resolution”, pp. 31-32, 2002.

[8] International standard ISO 12233 “Photography - Electronic still-picture cameras - Resolution measurements”, 2000.

[9] http://www.mathworks.com/matlabcentral/fileexchange/28631-slant-edge-script, retrieved February 23rd, 2012.